Available online at www.sciencedirect.com

ScienceDirect

Energy Procedia 94 (2016) 115 – 123

Energy Procedia

13th Deep Sea Offshore Wind R&D Conference, EERA DeepWind'2016, 20-22 January 2016, Trondheim, Norway

Effect of load sequence and weather seasonality on fatigue crack growth for monopile-based offshore wind turbines

Lisa Ziegler[a,b]*, Sebastian Schafhirt[b], Matti Scheu[a] and Michael Muskulus[b]

[a]*Rambøll, Wind & Towers, Stadtdeich 7, 20097 Hamburg, Germany*
[b]*Norwegian University of Science and Technology, Department of Civil and Transport Engineering, Høgskoleringen 7a, 7491 Trondheim, Norway*

Abstract

Offshore wind turbines are subjected to variable amplitude loading, but the impact of load sequence is commonly neglected in fatigue analysis. This paper presents an initial investigation if load sequence and weather seasonality influence fatigue crack growth for monopile-based offshore wind turbines. Focus is on the load sequence effect introduced by the non-linearity of crack propagation. Fatigue crack growth at two structural hot spots was analyzed with a fracture mechanics model applying Paris' law. The model was calibrated to yield an identical lifetime as a SN-curve analysis. Input into the fracture mechanics model are structural stresses due to environmental and operational loading. Weather seasonality was simulated with a Markov model. Results show that loading sequence has only a negligible effect on crack sizes under the assumption made in this study. This makes fatigue lifetime predictions independent of weather seasonality. However, it becomes relevant for the prediction of future propagation of detected fatigue cracks throughout the year.

Peer-review under responsibility of SINTEF Energi AS

Keywords: offshore wind turbine; fatigue crack growth; seasonality; sequence; fracture mechanics

1. Introduction

In the coming years, the first larger offshore wind farms approach the end of their design lifetime, which is typically limited to 20-25 years. An extension of the operation of aging wind farms beyond their design lifetime

* Corresponding author. Tel.: +49 151 44 006 445
E-mail address: lisa.ziegler@ramboll.com

Peer-review under responsibility of SINTEF Energi AS
doi:10.1016/j.egypro.2016.09.204

enables to increase the return on investment of wind projects. To decide whether a safe and economical operation extension is feasible, precise assessment of the remaining useful lifetimes of all offshore wind turbine (OWT) components is needed [1]. A crucial factor for lifetime extension is structural integrity of support structures.

Offshore wind monopiles are the predominant support structures installed in shallow and intermediate water depths [2]. The design of monopiles is often fatigue-driven as OWTs are exposed to long-term, variable-amplitude aerodynamic and hydrodynamic loading. Large uncertainties in environmental loading, material resistance, and design models cause that physical properties (and consequently lifetimes) of installed OWTs often differ from design assumptions [3]. For example, Kallehave et al [4] point out that the first natural frequency of monopiles is in general under-predicted in design (up to 20%). Fatigue lifetime calculations must therefore be updated with information from on-site inspections and monitoring data. In the offshore wind industry, damage calculation with SN-curves is commonly applied for fatigue design as recommended in relevant design standards [5,6]. SN-curves specify number of cycles until material failure (often defined as through-thickness crack) at a certain stress range, but miss out on description of propagation of fatigue cracks. Fracture mechanics approaches are suitable for lifetime updating based on crack inspections, since they depict all fatigue stages: crack initiation, crack propagation, and brittle fracture.

Linear-elastic fracture mechanics models have often been applied for tubular joints in the oil & gas industry [7-9]. However, there is only very limited literature available regarding crack propagation in welding types applicable to monopiles: circumferential butt welds, welded from both sides [5]. Lotsberg [10] derives stress concentration factors for circumferential welds in tubulars based on classical shell theory. Later, fatigue reliability and crack growth in circumferential butt welds of berthing monopiles was discussed by Li et al [11]. The effect of welding sequence on residual stress distribution in offshore wind monopiles was recently analysed by Mehmanparast et al. [12]. Their study concluded that residual stress profiles have to be measured at relevant support structure welds in order to predict crack growth accurately. To the knowledge of the authors, there is no published work that addresses linear-elastic fracture mechanic models for crack propagation in offshore wind monopiles. However, there is some work on crack growth in jacket structures mostly focusing on fatigue reliability [13] and risk-based inspection and maintenance planning [14-16].

Several fatigue experiments with materials exposed to variable amplitude loading have shown that large amplitude loads lead to a retardation of subsequent crack growth which is explained with a crack-closure or crack-tip plasticity theory [17-19]. Verma & Pandey [18] argued that the sequence, in which loading occurs on a structure, can influence the fatigue lifetime of the structure. As an example, Wheeler [19] established a retardation parameter which incorporates the effect of the crack tip yield zone into linear cumulative crack growth models. These effects are not captured in typical engineering models for crack propagation, e.g. Paris' law. However, load sequence might still influence results of the simplified engineering models due to the non-linearity of crack propagation. Both load sequence effects are currently neglected in published offshore wind research and industry practices.

This paper investigates if loading sequences introduced through (i) randomness of simulated load time series and (ii) weather seasonality have an impact on crack growth for a monopile-based OWT. Only fatigue relevant load cases (power production and idling) are modelled in this initial study, while ultimate loads are not considered. The analysis focuses on the sequence effect within the engineering model of Paris' law. The effect of crack retardation due to overloads is not accounted for. In addition, the model for fatigue crack propagation is simplified in many aspects. For example, the analytical formulation of Paris' law is applied but no attention is given to detailed modelling of stress intensity factors.

The remainder of this paper is organized as follows. Section 2 presents the fatigue crack propagation model used in the analysis, followed by an outline of the numerical support structure model and load simulations. In Section 3 the Markov weather model is introduced. Fatigue crack growth results are discussed in Section 4 and concluded in Section 5.

2. Fatigue crack growth

2.1. Fracture mechanics model

The fatigue life of a structure consists of (1) crack initiation through microstructural processes, (2) crack propagation, and (3) brittle fracture after accelerated crack growth [20]. Welded materials spent most of their

lifetime in the second phase of crack propagation due to the presence of small defects caused in the welding process, high local stresses at the weld, and high tensile residual stresses [20]. Continuous crack propagation can be described with linear-elastic fracture mechanics models. Paris' law [21] is a simple and commonly applied crack propagation model (cf. Equation 1 and 2). The change of crack size *da* per load cycle *dN* is a function of the stress intensity factor ΔK_I and two material constants *C* and *m*.

$$\frac{da}{dN} = C(\Delta K_I)^m \tag{1}$$

The stress intensity factor ΔK_I is calculated as a function of stress ranges ΔS (specific for the considered crack opening mode) and a geometry factor *Y* (cf. Equation 2). The geometry factor accounts for structural and crack geometry. Ideally, ΔS and *Y* are derived problem-specific with finite element models, however less involved analytical solutions are also provided by standards [22]. In this analysis, stresses are calculated as maximum principal stresses according to DNVGL [6].

$$\Delta K_I = \Delta S \cdot Y \sqrt{\pi \cdot a} \tag{2}$$

Recommended values (mean and standard deviation) for the material constants *C* and *m* are given in offshore standards based on experimental data [5,6,22]. Ziegler and Muskulus [23] give on overview about values that were applied by researchers for OWT jackets; however experiences regarding circumferential butt welds for offshore wind monopiles are still missing. Alternatively, *C* and *m* can be treated as model parameters which are calibrated with results from SN-curve analysis. For example, Sørensen [14] calibrates his fracture mechanics model to yield the same reliability level over time as calculated with linear damage accumulation based on SN-curves. A semi-empirical approach is used here to calibrate *C* so that the crack depth *a* reaches the critical crack depth a_c after $T_{failure}$ [23]. The critical crack depth a_c represents fatigue failure expressed by a through-thickness crack (a_c equals material wall thickness). $T_{failure}$ is the time until failure (damage = 1) calculated with the SN-curve analysis. SN-curve parameters from detail category "D" with corrosion protection and thickness correction were applied [5]. In addition, Table 1 specifies the crack growth parameters used in this study. No threshold value was applied for the stress intensity factor. The initial crack depth depends on welding mechanisms which inevitably introduce small material defects.

Table 1. Parameters applied in the crack propagation analysis. Some values differ in the analysis of welds at mudline (ML) and tower bottom (TB).

Parameter	Unit	Value ML / TB	Source
Initial crack depth a_0	mm	0.1	[5]
Critical crack depth a_c	mm	60 / 27	[11,13]
Material parameter *m*	-	3.1	[5]
Material parameter *ln(C)*	$mm(MPa\sqrt{mm})^{-m}$	-28.36 / -28.52	calibrated
Geometry factor *Y*	-	1	[7]

Table 2. Dimensions of OC3 monopile and tower [24].

	Tower top	Tower bottom	Monopile
Diameter [m]	3.87	6.0	6.0
Wall thickness [m]	0.019	0.027	0.06

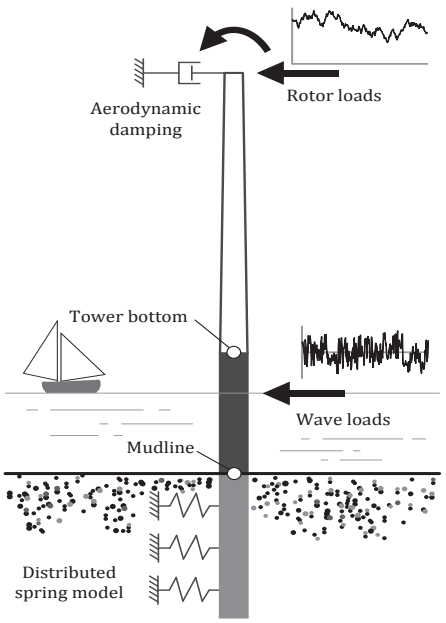

Fig 1. Model of monopile used in this study.

2.2. Numerical model of OC3 monopile and load simulations

The study was performed with the generic OWT used during Phase II of the OC3 project [24]. This OWT is located in 20 m water depth and consists of a monopile and the NREL 5MW reference turbine atop [25]. Soil-pile interaction was represented with a distributed spring model adopted from Passon [26]. Figure 1 illustrates the numerical model of the monopile-based OWT including the distinct output locations. Structural dimensions are given in Table 2. Structural response to aero- and hydrodynamic loading is evaluated at two locations: tower bottom and mudline (cf. Figure 1).

Load analyses were performed for two different load cases in accordance with the IEC standard [27], representing the most important design situations for fatigue: power production and idling. In total 15 load situations were defined according to the wind speed distribution presented in Figure 2b: from 2-30 m/s in steps of 2 m/s. The OWT is in operation for the wind speeds 4-24 m/s, and in idling for other wind speeds. Environmental conditions, such as lumped sea states and turbulence intensities, were taken from the UpWind Design Basis [28]. Currents and yaw-misalignment were neglected in the simulation. The simulation time was 1h for each load situation.

In order to speed up the analysis, the simulation of aerodynamic and hydrodynamic loads was performed decoupled from each other in the structural analysis [29]. A standalone bottom-fixed rotor model was used to obtain time series for forces and moments acting on the top of the support structure. Time series for wave forces were derived from time-domain simulations of a vertical cylinder. They are applied during the simulation at mean sea level and adapted in order to produce a bending moment at ML equivalent to the original time-domain simulations. The decoupling of the rotor simulation neglects the dynamic interaction between rotor and support structure. Therefore, a viscous damper was implemented on the top of the support structure to account for the effect of aerodynamic damping [30].

Structural response was calculated with impulse based substructuring [31,32]. In this approach, the dynamics of the support structure are represented by impulse response functions. For structural analysis of the offshore wind monopile the impulse response functions are determined by applying small impulse loads in six degrees of freedom on the top of the structural model (to account for rotor loads) and in one degree of freedom at mean sea level (to account for wave loads). The response of the structure at TB and ML is then calculated by convolution of the impulse response function with the load time series from rotor and waves. It was shown that this approach leads to accurate results [29,31] and a recent implementation using a general purpose graphic processing unit turns it into a highly efficient load analysis method [29].

3. Weather seasonality and sequence effects

3.1. Markov weather model

For the load sequence analysis a weather model is required that (i) enables a realistic representation of the absolute wind and wave distributions, (ii) covers seasonal trends and (iii) reproduces persistence of weather phenomena. Markov chains, which describe stochastic processes with finite memory, are suitable for this purpose [33]. In this paper, a Markov model is used to simulate a discrete wind time series with the duration of the structural lifetime and 6 h time steps [34]. Wind speeds are discretized in bins of 2 m/s from 2-30 m/s according to the load situations defined in Section 2.2. Wave conditions are lumped and allocated to each wind speed as specified in the UpWind Design Basis [28] in order to reduce the number of load simulation.

The Markovian transition matrix T_M specifies the transition probabilities p_{ij} that one wind speed i turns into the wind speed j in the next time interval (cf. Equation 3). This transition matrix is set up from historical wind data.

$$T_M = \begin{bmatrix} p_{11} & p_{12} & \cdots & p_{1s} \\ p_{21} & p_{22} & \cdots & p_{2s} \\ \cdots & \cdots & \cdots & \cdots \\ p_{s1} & p_{s2} & \cdots & p_{ss} \end{bmatrix} \tag{3}$$

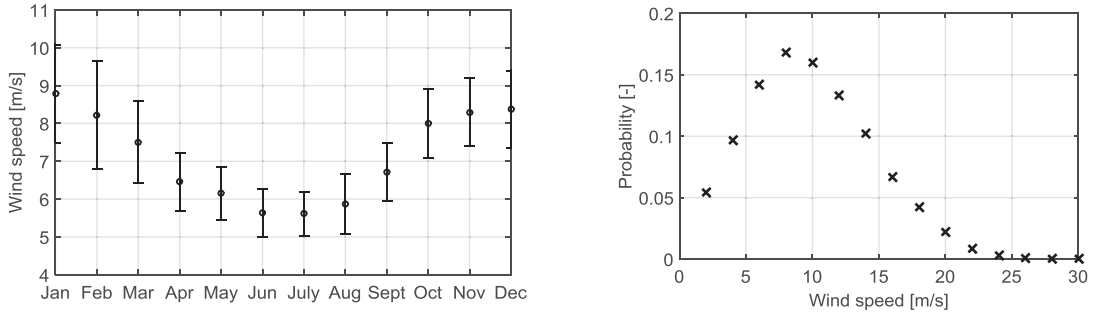

Fig. 2. (a) Monthly variation of wind speed from 22 years of historical data. Error bars indicate the standard deviation; (b) Probability of occurrence of wind speed bins derived from the historical data.

For this paper, 22-years of hindcasted wind data with 6 h resolution from a location in the North Sea near the UK cost provided by the European Center for Medium-Range Weather Forecasts [35] were employed. Markov matrices are calculated monthly, so that weather seasonality throughout the year is reproduced. The weather seasonality present in the historical data is shown in Figure 2a: the monthly mean wind speeds can differ over 3 m/s from summer to winter. Further details of the applied Markov model can be found in [34].

3.2. Simulation of realistic loading sequence

The Markov weather model is used to simulate wind conditions that occur during the lifetime of the investigated structural hot spots (SN-curve based lifetime calculation). The load situations that match the wind conditions (cf. Section 2.2) were ordered in the sequence of the simulated wind time series – leading to a realistic, time-dependent loading sequence. Rainflow counting displays the stress ranges ΔS_i that are then applied in Equation 1 and 2.

In Equation 1, the crack growth increment *da/dN* at time step *i* depends on the crack size of the previous time step *i-1*. This could lead to an impact of the order of load amplitudes on crack development. In the following analysis, a realistic load sequence is compared to loads sorted (i) ascending and (ii) descending. The sorted loads are expected to yield the boundaries of the crack growth sample space.

4. Results and Discussion

4.1. Calibration of crack growth model

Figure 3a presents the stress ranges at TB and ML scaled to 20 years of lifetime and the corresponding SN-curves (detail category “D” and corrected for material thickness). The resulting damage values after 20 years and linearly

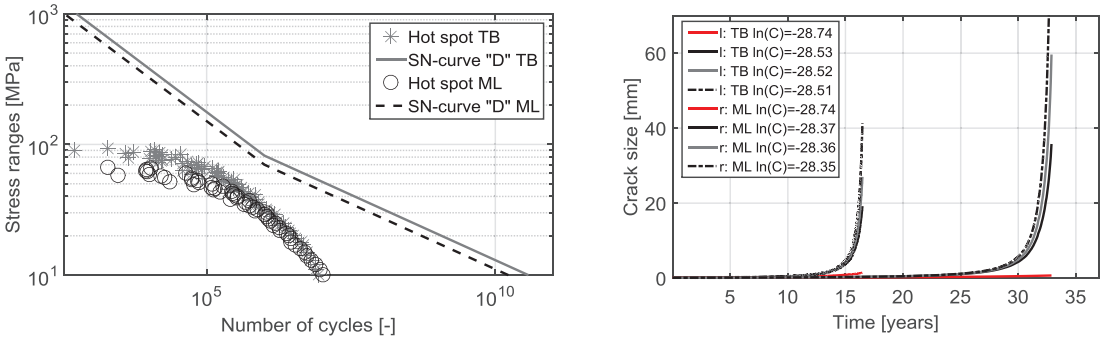

Fig. 3. (a) SN-curves detail category “D” corrected for material thickness. Numbers of cycles of stress ranges for 20 year lifetime are plotted for TB and ML; (b) Crack growth at TB (l curves) and ML (r curves) for various *C* parameters during the hot spot lifetime with random weather occurrence. The grey lines correspond to the calibrated *C* value, while the red lines are the *C* values recommended in DNV [5].

extrapolated lifetimes are given in Table 3. Linear extrapolation is possible due to the linear damage accumulation hypothesis (Miners rule) used in the SN-curve calculation. The damage at TB is larger than 1.0 resulting in a reduced lifetime of 16.48 years. This shows that the design does not fulfill requirements for this site.

Table 3. Damage values and extrapolated lifetime from the SN-curve calculation and calibrated *C* parameter for the fracture mechanics model.

Location	20 year damage [-]	lifetime for $D=1$ [years]	$ln(C)$ [$_{mm(MPa\sqrt{mm})^{-m}}$]
Tower bottom	1.21	16.48	-28.52
Mudline	0.61	32.89	-28.36

The sensitivity of crack growth results to variation in *C* in the fracture mechanics model is presented in Figure 3b. The grey lines show the crack propagation with the calibrated C parameters which results in a through-thickness crack after 16.48 years and 32.89 years (time until D=1 from SN-curve analysis, see Table 3). Results of the C parameters calibration are stated in Table 3. The red line in Figure 3b gives the crack propagation using recommended material values from DNV [5]. The calibration results for *C* (grey line) are more conservative than the recommended material values (red line). The influence of *C* is stronger to the end of the structural life, where small deviations influence the crack growth, while crack growth at crack sizes below 5mm earlier in the lifetime is insensitive to applied variations of *C*.

4.2. Effect of loading sequence and weather seasonality

The effect of loading sequence on fatigue crack growth is analyzed for a six hour time interval in Figure 4a and for the complete lifetime in Figure 4b (example ML hot spot). Stress ranges of one load situation are sorted in ascending and descending order and the resulting crack growth is compared to the random stress order in Figure 4a. The initial crack size was taken as 10mm. The crack growth rates within the time interval are initially higher and decelerate later for descending loads and vice versa, as expected. However, it is important that the total increase in crack depth within this six hour interval is identical for both sorted as well as random load order (absolute difference is smaller than numerical errors). This behavior is identical on various time scales: day, month, year, and lifetime. As an example, the results for the lifetime scale are presented in Figure 4b. Crack growth starts from an initial crack size of 0.1mm as a function of the stress ranges in ascending and descending order over time. In addition, the numbers of cycles per stress range are plotted in red. The crack growth accelerates independent of sorting towards the end of the lifetime, so that for ascending loads the stress ranges with higher amplitude contribute most to crack growth while for descending loads the lower stress ranges contribute more. Both loading orders end at a final crack depth that only differs minimally from the third decimal place on.

The lack of an effect of loading sequence on the final crack depth can be attributed to the dominance of low amplitude stress ranges (cf. Figure 4b, red line). In a separate analysis, loads a factor 10 higher were applied in the

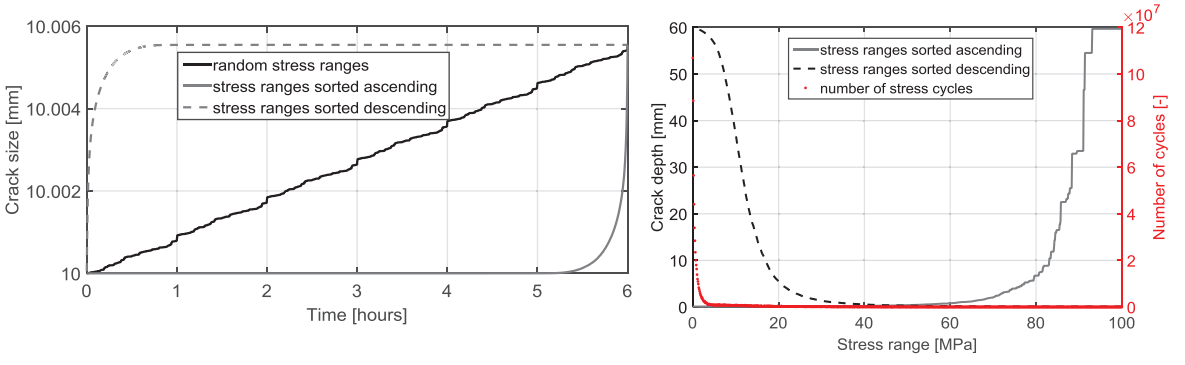

Fig. 4. (a) Crack growth for a six hour time interval for the ML hot spot assuming an initial crack size of 10 mm. Crack growth is compared for stress ranges in random, descending and ascending order; (b) Crack growth for the structural lifetime, calculated with (i) ascending and (ii) descending stress order, is plotted as a function of the stress ranges. The numbers of cycles per stress range are added in red.

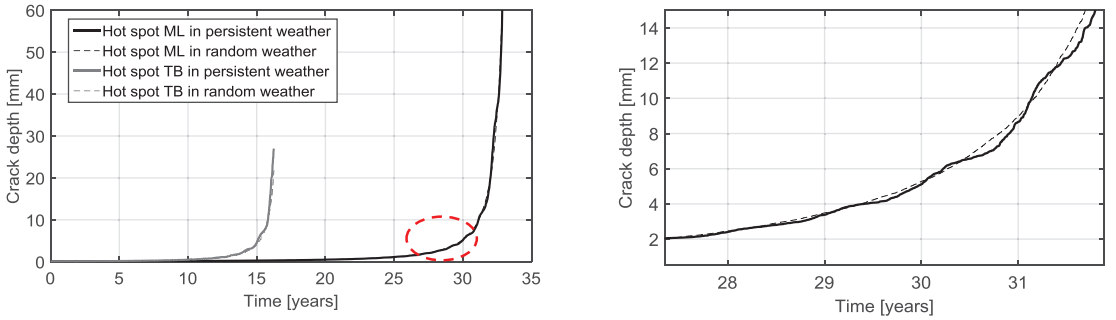

Fig. 5. (a) Comparison of crack growth at ML and TB hot spots from persistent weather simulations and random weather occurrence; (b) Zoom into the red-marked area in Figure 5a for visualization. Crack growth follows annual weather seasonality.

crack growth model. These hypothetical loads led to a 5.3% higher final crack size for descending load order compared to ascending load order in a six hour time interval (not shown here). In this case the random stress order would result in 2.7% higher final crack size compared to the ascending sorted loads. This indicates that ultimate loads might have an influence on the fatigue crack propagation, although fatigue design is treated isolated from ultimate load analysis in current offshore wind practice.

Results of the weather seasonality analysis are in line with the previous study: there is only a negligible effect on the final crack depth. However, seasonal weather trends are clearly visible in the crack growth rates closer to the end of structural lifetime (cf. Figure 5). In Figure 5, crack growth due to a persistent weather simulation (with seasonality) is compared to an identical wind speed occurrence but randomized in order (no persistence, no seasonality). Figure 5b is a zoom into the area marked red in Figure 5a. Crack growth follows weather seasonality: it accelerates from autumn to spring and retards in the other half of the year. This is caused by higher wind speeds in winter than in summer time. This seasonality effects can become relevant for answering questions about a detected fatigue crack close to the end of structural life, such as:

- How much does the detected fatigue crack propagate until the next scheduled inspection?
- Must the crack be repaired or will it not develop to a critical size during the remaining service life?

The relevance of the seasonality effect is limited by the uncertainty in sizing of a detected fatigue crack for specific inspection technique. As an example, according to DNVGL [36] the sizing error for an indicated 1 mm deep crack in a butt weld of an offshore jacket is accounted for with a standard deviation of 0.5 mm for an eddy current inspection method. Compared to this assumption, the crack depth differences due to weather seasonality partly exceed the sizing uncertainty (cf. Figure 5b).

5. Conclusion and Outlook

The effect of load sequence and weather seasonality on fatigue crack growth was studied with a simplified crack propagation model applying Paris' law. Results for a monopile-based 5MW OWT in 20m water depth indicate that loading sequence does not influence the long-term crack size development considering fatigue relevant load cases only. Weather seasonality causes likewise only negligible differences in structural lifetimes. However, throughout a year the acceleration of crack growth during winter and retardation during summer can become relevant for predictions regarding the future propagation of detected fatigue cracks.

Concerning the question of lifetime extension, this study indicates - under the assumption made - that it is not necessary to reassess lifetime calculations in terms of occurred fatigue load sequence. The common procedure of neglecting sequence effects in monopile design seems appropriate for the studied reference case. However, it is strongly emphasized that this is only an initial study with major simplifications in the fracture mechanics model. Additionally, the analysis does not consider the physical effect of crack retardation due to overload, which can significantly change the importance of load sequence. Further research is needed to implement crack growth retardation phenomena for offshore wind monopiles and to evaluate the impact of ultimate loads on fatigue lifetime.

Acknowledgements

This project has received funding from the European Union's Horizon 2020 research and innovation programme under the Marie Sklodowska-Curie grant agreement No 642108. Additional support by the Norwegian Research Centre for Offshore Wind Technology (NOWITECH FME; Research Council of Norway Contract No. 193823) is gratefully acknowledged.

References

[1] Faber T, & Hansen K. 2010. First guideline for the continued operation of wind turbines. *Steel Construction, 3*, 56–59.
[2] Corbetta G, Pineda I, Moccia J, & Guillet J. 2014. The European offshore wind industry - key trends and statistics 2013. Report. Brussels: European Wind Energy Association.
[3] Ziegler L, Voormeeren S, Schafhirt S, & Muskulus M. 2016. Design clustering of offshore wind turbines using probabilistic fatigue load estimation. *Renewable Energy*. DOI: 10.1016/j.renene.2016.01.033.
[4] Kallehave D, Byrne BW, LeBlanc Thilsted C, & Mikkelsen KK. 2015. Optimization of monopiles for offshore wind turbines. *Phil. Trans. R. Soc. A, 373*, 20140100. http://dx.doi.org/10.1098/rsta.2014.0100.
[5] DNV. 2014. Design of offshore wind turbine structures. Offshore standard DNV-OS-J101. Høvik: Det Norske Veritas.
[6] DNVGL. 2014. Fatigue design of offshore steel structures. Recommended practice RP-C203.
[7] Kirkemo F. 1988. Applications of probabilistic fracture mechanics to offshore structures. *Applied Mechanics Reviews, 41*(2), 61-84.
[8] Shetty NK, & Baker MJ. 1990a. Fatigue reliability of tubular joints in offshore structures: Crack propagation model. *Proc., Int. Offshore Mechanics and Arctic Eng. Symposium, ASME, 2:* 223–230.
[9] Qian X. 2016. Fracture representation and assessment for tubular offshore structures. In: *Handbook of Materials Failure Analysis with Case Studies from the Oil and Gas Industry.* Elsevier, pp. 371–392.
[10] Lotsberg I. 1998. Stress concentration factors at circumferential welds in tubulars. *Mar. Struct., 11*(6), 207–230.
[11] Li Y, Lence BJ, Shi-Liang Z, & Wu Q. 2011. Stochastic Fatigue Assessment for Berthing Monopiles in Inland Waterways. *J. Waterway, Port, Coastal, Ocean Eng, 137* (2): 43–53. DOI: 10.1061/(ASCE)WW.1943-5460.0000063.
[12] Mehmanparast A, Adedipe O, Brennan F, & Chahardehi A. 2015. Welding sequence effects on residual stress distribution in offshore wind monopile structures. *Fracture and Structural Integrity, 35:* 125-131. ISSN 19718993.
[13] Dong W, Moan T, & Gao, Z. 2012. Fatigue reliability analysis of the jacket support structure for offshore wind turbine considering the effect of corrosion and inspection. *Reliability Engineering and System Safety, 106*: 11-27.
[14] Sørensen JD. 2009. Framework for risk-based planning of operation and maintenance for offshore wind turbines. *Wind Energy, 12:* 493–506.
[15] Rangel-Ramírez JG. 2010. Reliability Assessment and Reliability-Based Inspection and Maintenance of Offshore Wind Turbines. *PhD thesis,* Aalborg University, Denmark.
[16] Nielsen JS. 2013. Risk-based operation and maintenance of offshore wind turbines. *PhD thesis*, Aalborg University, Denmark.
[17] Lee SY, Sun Y, An K, Choo H, Hubbard CR, & Liaw PK. 2010. Evolution of residual-strain distribution through an overload-induced retardation period during fatigue-crack growth. In *J. Appl. Phys. 107* (2), p. 23517. DOI: 10.1063/1.3234388.
[18] Verma BB, & Pandey RK. 1999. The effects of loading variables on overload induced fatigue crack growth retardation parameters. In *Journal of Materials Science 34* (19): 4867–4871. DOI: 10.1023/A:1004624213382.
[19] Wheeler OE. 1972. Spectrum loading and crack growth. *Journal of Fluids Engineering, 94*(1): 181-186.
[20] Stephens RI, & Fuchs HO. 2000. *Metal fatigue in engineering*. 2nd ed. New York: J. Wiley.
[21] Paris P, & Erdogan F. 1963. A critical analysis of crack propagation laws, *Journal of Basic Engineering, Trans. ASME (85)*: 528-534.
[22] BS. 2005. *Guide on methods for assessing the acceptability of flaws in fusion welded structures.* British Standard 7910. London: British Standard Institutions.
[23] Ziegler L, & Muskulus M. 2016. Comparing a fracture mechanics model to the SN-curve approach for jacket-supported offshore wind turbines: Challenges and opportunities for lifetime prediction. *35th International Conference on Ocean, Offshore and Arctic Engineering: Ocean Renewable Energy*, Busan, Korea.
[24] Jonkman J, & Musial W. 2010. Offshore code comparison collaboration (OC3) for IEA task 23 offshore wind technology and deployment. *Technical report*, Golden, CO: National Renewable Energy Laboratory.
[25] Butterfield S, Musial W, & Scott G. 2009. Definition of a 5-MW reference wind turbine for offshore system development. Golden, CO: National Renewable Energy Laboratory.
[26] Passon P. 2006. Derivation and description of the soil-pile-interaction models. University of Stuttgart, Germany, IEA-Annex, 23.
[27] IEC. 2009. *Wind turbines – part 3: Design requirements for offshore wind turbines.* International standard IEC 61400-3. Geneva: International Electrotechnical Commission.
[28] Fischer T, De Vries WE, & Schmidt B. 2010. *UpWind design basis (WP4: Offshore foundations and support structures).* Upwind.
[29] Schafhirt S, Verkaik N, Salman Y, & Muskulus M. 2015. Ultra-fast analysis of offshore wind turbine support structures using impulse based substructuring and massively parallel processors. *Proc 25th International Ocean and Polar Engineering Conference (ISOPE2015).*
[30] Salzmann DJC, & Van der Tempel J. 2005. Aerodynamic damping in the design of offshore support structures for offshore wind turbines. *Proc. European Offshore Wind Conference Copenhagen.* Brussels: European Wind Energy Association.

[31] Rixen DJ. 2011. Substructuring using impulse response functions for impact analysis. In *Structural Dynamics, Volume 3* (pp. 637-646). Springer New York.
[32] Van der Valk PLC, & Rixen DJ. 2012. Impulse based substructuring for coupling offshore structures and wind turbines in aero-elastic simulations. *Proceedings of 53rd AIAA/ASME/ASCE/AHS/ASC Structures, Structural Dynamics and Materials Conference*, 23 - 26 April 2012, Honolulu, Hawaii.
[33] Anastasiou K, & Tsekos C. 1996. Persistence statistics of marine environmental parameters from Markov theory, Part 1: Analysis in discrete time. *Appl. Ocean Res., 18*:187-199.
[34] Scheu M, Matha D, & Muskulus M. 2012. Validation of a Markov-based weather model for Simulation of O&M for Offshore Wind Farms. *Proceedings of the 22th International Offshore and Polar Engineering Conference,* 463-368.
[35] ECMWF. 2011. Homepage of European Centre for Medium-Range Weather Forecasts: www.ecmwf.int. Accessed on 21/11/2011.
[36] DNVGL. 2015. Probabilistic methods for planning of inspection for fatigue cracks in offshore structures. Recommended practice RP-0001.